Contribution from the Department of Chemistry,
University of Minnesota, Minneapolis, Minnesota 55455

Chemical, Electrochemical, and Structural Properties of Some Novel Dithiocarbamato Complexes of Osmium(IV)

S. H. WHEELER and L. H. PIGNOLET*

Received July 25, 1979

The complex tris(*N*,*N*-diethyldithiocarbamato)osmium(IV) hexafluorophosphate, $[Os(dtc)_3]PF_6$, has been synthesized and characterized and found to exhibit a novel monomer–dimer equilibrium in CH_2Cl_2 solution: $2[Os(dtc)_3]^+ \rightleftarrows [Os_2(dtc)_6]^{2+}$. The ^1H NMR and electrochemical properties of this complex have been studied as a function of temperature in CH_2Cl_2 solution. The monomer and dimer species are observed electrochemically only at −78 °C where the equilibrium is established slowly. The equilibrium is slow on the ^1H NMR time scale at temperatures below 25 °C. $[Os(dtc)_3]^+$ rapidly reacts with donor ligands such as CH_3CN and Cl^- forming the diamagnetic seven-coordinate complexes $[(CH_3CN)Os(dtc)_3]^+$ and $ClOs(dtc)_3$, respectively. The latter complex is partially dissociated into $[Os(dtc)_3]^+$ and Cl^- in propylene carbonate solution. The electrochemistry of $ClOs(dtc)_3$ has been examined in this solvent as a function of temperature. The crystal and molecular structure of the dimer $[Os_2(dtc)_6](PF_6)_2$ has been determined by single-crystal X-ray methods by using an automatic diffractometer. The compound crystallizes as a CH_2Cl_2 solvate in the space group $P\bar{1}$ with unit cell dimensions a = 15.162 (8) Å, b = 15.539 (6) Å, c = 13.556 (7) Å, α = 98.20 (4)°, β = 107.65 (4)°, γ = 88.57 (4)°, and V = 3012 Å^3 with Z = 2. Refinement by full-matrix least-squares methods (409 variables, 6017 observations) converged to a final R value of 0.052. The structure consists of dimers of $[Os(dtc)_3]^+$. The geometry about each Os atom is that of a distorted pentagonal bypyramid (PBP) with one axial position occupied by a bridging sulfur atom (of a dtc ligand) which also occupies the equatorial plane of the PBP of the other Os atom. The average Os–S distance is 2.415 (3) Å, and the Os–Os distance of 3.682 (1) Å indicates no metal–metal bonding.

Introduction

The redox chemistry of iron, ruthenium, and osmium tris(*N*,*N*-dialkyldithiocarbamates), $M(dtc)_3$, has been the subject of many recent publications.[1-12] Interest in this area stems from the potential usefulness of these complexes as photoredox catalysts[7,13-15] and from the novel structural chemistry which has thus far been unraveled.[2,5,6,8,16] Additionally, metal dithiocarbamato complexes have been shown to be effective accelerators in the vulcanization of rubber,[17,18] and the recent characterization of a sulfur-rich dtc complex of osmium is especially relevant.[2]

Oxidation of $M(dtc)_3$ complexes has been achieved electrochemically by controlled-potential electrolysis and by the novel quantitative reaction with BF_3 gas under aerobic conditions. With iron(III), both reactions yield the stable cationic paramagnetic tris-chelate complex of iron(IV) as shown by eq 1.[10,12] The chemistry is quite different with ruthenium(III)

$$Fe(dtc)_3 \xrightarrow{-e^-,\ CH_3CN} [Fe(dtc)_3]^+ \qquad (1a)$$

$$Fe(dtc)_3 \xrightarrow[\text{benzene}]{BF_3/O_2} [Fe(dtc)_3]BF_4 \qquad (1b)$$

as shown by eq 2. The products of reactions 2a–c are diamagnetic and have the following structures.

$$Ru(dtc)_3 \xrightarrow{-e^-,\ CH_3CN} [(CH_3CN)Ru(dtc)_3]^+ \qquad (2a)$$

$$Ru(dtc)_3 \xrightarrow[\text{benzene}]{BF_3/O_2} \beta[Ru_2(dtc)_2]BF_4 \qquad (2b)$$

$$Ru(dtc)_3 \xrightarrow[\text{benzene}]{BF_3/N_2} \alpha[Ru_2(dtc)_5]BF_4 \qquad (2c)$$

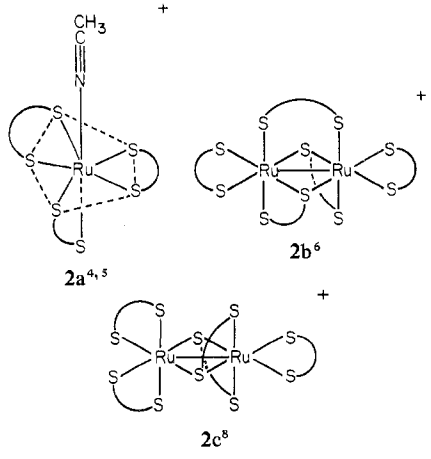

2a[4,5]

2b[6]

2c[8]

Reactions 2b and 2c do *not* represent ruthenium oxidations since the products contain Ru(III); however, in reaction 2b the lost Et_2dtc is oxidized to [3,5-bis(*N*,*N*-diethyliminium)-1,2,4-trithiolane]$^{2+}$.[6] The origin of the difference in stereochemistry between reactions 2b and 2c is not understood;[4] however, 2c is rapidly converted into 2b in solution by treatment with BF_3/O_2 or slowly by heating.[4,11] The analogous chemistry of osmium(III) partially resembles that of iron as

(1) Given, K. W.; Wheeler, S. H.; Jick, B. S.; Maheu, L. J.; Pignolet, L. H. *Inorg. Chem.* **1979**, *18*, 1261.
(2) Maheu, L. J.; Pignolet, L. H. *Inorg. Chem.*, **1979**, *18*, 3626.
(3) Dix, A. H.; Diesveld, J. W.; van der Linden, J. G. M. *Inorg. Chim. Acta* **1977**, *24*, L51.
(4) Wheeler, S. H.; Mattson, B. M.; Miessler, G. L., Pignolet, L. H. *Inorg. Chem.* **1978**, *17*, 340.
(5) Given, K. W.; Mattson, B. M.; Pignolet, L. H. *Inorg. Chem.* **1976**, *15*, 3152.
(6) Mattson, B. M.; Heiman, J. R.; Pignolet, L. H. *Inorg. Chem.* **1976**, *15*, 564.
(7) Miessler, G. L.; Zoebisch, E.; Pignolet, L. H. *Inorg. Chem.* **1978**, *17*, 3636.
(8) Raston, C. L.; White, A. H. *J. Chem. Soc., Dalton Trans.* **1975**, 2410.
(9) McCleverty, J. A.; McLuckie, S.; Morrison, N. J.; Bailey, N. A.; Walker, N. W. *J. Chem. Soc., Dalton Trans.* **1977**, 359.
(10) Pasek, E. A.; Straub, D. K. *Inorg. Chem.* **1972**, *11*, 259.
(11) Hendrickson, A. R.; Hope, J. M.; Martin, R. L. *J. Chem. Soc., Dalton Trans.* **1976**, 2032.
(12) Chant, R.; Hendrickson, A. R.; Martin, R. L.; Rohde, N. M. *Inorg. Chem.* **1975**, *14*, 1894.
(13) Miessler, G. L.; Pignolet, L. H. *Inorg. Chem.* **1979**, *18*, 210.
(14) Given, K. W.; Mattson, B. M.; McGuiggan, M. F.; Miessler, G. L.; Pignolet, L. H. *J. Am. Chem. Soc.* **1977**, *99*, 4855.
(15) Schwendiman, D. P.; Zink, J. I. *J. Am. Chem. Soc.* **1976**, *98*, 4439. Liu, P. H.; Zink, J. I. *Ibid.* **1977**, *99*, 2155.
(16) Given, K. W.; Pignolet, L. H. *Inorg. Chem.* **1977**, *16*, 2982.
(17) Coleman, N. M.; Shelton, J. R.; Koenig, J. L. *Ind. Eng. Chem. Prod. Res. Develop.* **1974**, *13*, 154.
(18) Allen, P. W.; Barnard, D.; Saville, B. *Chem. Br.* **1970**, *6*, 382.

0020-1669/80/1319-0972$01.00/0

shown by eq 3; however, the paramagnetic Os(IV) complex,

$$Os(dtc)_3 \xrightarrow[CH_2Cl_2]{-e^-} [Os(dtc)_3]^+ \quad (3a)$$

$$Os(dtc)_3 \xrightarrow[CH_2Cl_2]{BF_3/O_2} [Os(dtc)_3]BF_4 \quad (3b)$$

$[Os(dtc)_3]^+$, readily reacts with donors such as CH_3CN and Cl^- yielding seven-coordinated diamagnetic complexes $(X)Os(dtc)_3^+$, where X = donor, analogous to **2a**.[1] Additionally, Os(III) complexes similar to Ru compounds **2b** and **2c** have been synthesized.[1,19] Compounds **2a–c** *cannot* be made with iron. $[Os(dtc)_3]^+$, where dtc hereafter refers to *N,N*-diethyldithiocarbamate, exhibits a novel monomer–dimer equilibrium in CH_2Cl_2 solution as determined by ^1H NMR and electrochemical experiments and exists exclusively as a diagmagnetic dimer in the solid phase as determined by single-crystal X-ray diffraction. Details of the ^1H NMR and electrochemical experiments with $[Os(dtc)_3]^+$ and $ClOs(dtc)_3$ and of the X-ray structure of $[Os_2(dtc)_6](PF_6)_2$ will be presented in this paper.

Experimental Section

Synthesis of $[Os(dtc)_3]PF_6$. This complex was prepared by bubbling BF_3 gas through an aerobic CH_2Cl_2 solution of $Os(dtc)_3$[1] (0.01 M) for 30 s. The resulting purple solution was purged with N_2 to remove excess BF_3. A threefold molar excess of Et_4NPF_6 was added to the solution which was then extracted once with water. Heptane was added to the CH_2Cl_2 solution to precipitate any Et_4NBF_4 or Et_4NPF_6 which was not removed by the water extraction, and the solution was filtered through a fine glass frit. The filtrate was allowed to slowly evaporate in the dark giving dark brown needlelike crystals which were thoroughly washed with distilled water and dried in vacuo. The yield of pure $[Os(dtc)_3]PF_6$ was 70%: IR (KBr disk) $\nu(C{\cdots}N)$ 1525 cm^{-1}, $\nu(P—F)$ 841 cm^{-1}; conductivity in CH_2Cl_2 at 25 °C 59 Ω^{-1} cm^2 $equiv^{-1}$; mp 159–161 °C; magnetic data, diamagnetic in solid state (23 °C by Faraday method),[20] CH_2Cl_2 solution (by Evans' NMR method[21]) $\chi_M^{corr} = 772 \times 10^{-6}$ cgsu/mol (27 °C) giving $\mu_{eff} = 1.4\ \mu_B$ (diamagnetic correction = 385×10^{-6} cgsu/mol); electronic absorption spectrum recorded in propylene carbonate solution (λ_{max}, nm (log ϵ)) 253 (4.56), 344 (4.08), 361 (4.00, sh), 450 (3.48, sh), 499 (3.75), 543 (3.63, sh). A similar spectrum was observed in CH_2Cl_2 solution: 246 (4.54), 345 (4.20), 360 (4.08, sh), 460 (3.54, sh), 500 (3.81), 543 (3.66, sh). Anal. (Eisenhower) Calcd for $OsS_6C_{15}H_{30}N_3PF_6$: C, 23.10; H, 3.88; N, 5.39. Found: C, 23.42; H, 3.67; N, 5.49.

$Os(dtc)_3$ and $ClOs(dtc)_3$ were prepared as previously reported.[1]

Electrochemical Measurements. All measurements were made with a three-electrode Princeton Applied Research Model 170 instrument with a glassy carbon indicator electrode, a saturated calomel reference electrode (SCE), and platinum auxiliary electrode. A coil of heavy-gauge platinum wire was used as the electrode in electrolysis experiments. The SCE was separated from the sample compartment by three nonaqueous salt bridges connected by glass frits. Solutions were ca. 0.5–2 mM in complex, and tetrabutylammonium tetrafluoroborate (TBAF) was used as the supporting electrolyte in CH_2Cl_2 solution whereas tetraethylammonium perchlorate (TEAP) was used in propylene carbonate solution. All experiments were done under a nitrogen atmosphere at the indicated temperature. The cyclic voltammograms were recorded on an X-Y recorder at 50–200 mV s^{-1}. Burdick and Jackson "distilled in glass" methylene chloride and propylene carbonate ($C_4H_6O_3$) solvents were dried over molecular sieves and used without further purification. Eastman reagent grade TEAP was recrystallized six times from water and dried in vacuo. Eastman reagent grade TBAF was dissolved in CH_2Cl_2, stirred with activated charcoal and filtered through sand, and reprecipitated twice from methylene chloride/heptane solution. CH_2Cl_2 and $C_4H_6O_3$ solutions were 0.2 M in TBAF and TEAP, respectively.

Spectral and Other Measurements. Electronic absorption spectra were recorded with a Cary 14 spectrophotometer using 1-cm quartz cells. Infrared spectra were recorded on a Perkin-Elmer Model 237 grating instrument. ^1H NMR spectra were obtained on a Varian CFT 20 instrument. A Yellow Springs Instrument Co. Model 31 conductivity bridge was used for conductivity measurements. Complex concentrations used in the conductivity experiments were ca. 1×10^{-3} M. Solid-state magnetic measurements were made at 23 °C by use of the Faraday technique, and $Hg[Co(SCN)_4]$ was used as a calibrant.

Structure Determination. Good quality crystals of $[Os_2(dtc)_6](PF_6)_2 \cdot nCH_2Cl_2$ were obtained from CH_2Cl_2–heptane by the solvent diffusion technique. All crystals isolated were CH_2Cl_2 solvates which readily lost solvent upon removal from the mother liquor thus rendering them unsuitable for single-crystal X-ray analysis. Several usable crystals were mounted inside capillary tubes which were completely filled with mother liquor and sealed with epoxy resin. The first crystal examined belonged to the triclinic space group $P\bar{1}$. The unit cell dimensions were determined by least-squares refinement of the angular settings of 25 Mo Kα (λ = 0.71069 Å) peaks centered on a CAD4 diffractometer[22a] at ambient temperature and are a = 15.584 (6) Å, b = 15.723 (2) Å, c = 13.618 (3) Å, α = 98.65 (1)°, β = 108.83 (2)°, γ = 89.31 (2)°, and V = 3120 (3) Å^3. Only a partial data set (3536 unique reflections) was collected by using this crystal since a leak developed in the capillary and the crystal powdered. By use of 2536 reflections (complete data for one hemisphere for $0° < \theta \leq 15°$ and partial data for one hemisphere for $15° < \theta \leq 20°$) with $F_o^2 \geq 3.0\sigma(F_o^2)$ the structure was solved by conventional heavy-atom techniques.[22b] All nonhydrogen atoms were located and clearly showed the molecule to be the dimeric disolvate $[Os_2(dtc)_6](PF_6)_2 \cdot 2CH_2Cl_2$. Refinement by full-matrix least squares was not continued due to the limited data set and at this stage R = 0.145, R_w = 0.210 for 67 atoms, 279 variables, and 2536 observations.[23] The structure of the dictation is essentially the same as in the monosolvate (vide infra) and therefore the disolvated structure will not be discussed further.

The second crystal examined proved satisfactory for a complete structural determination. The dimensions of this crystal were 0.40 × 0.05 × 0.20 mm. The crystal class was determined to be triclinic and the centric space group $P\bar{1}$ (Z = 2) led to a successful solution and refinement. The unit cell dimensions were determined by least-squares refinement of the angular values of 25 Mo Kα peaks centered on a CAD4 diffractometer using the Enraf-Nonius automatic peak centering programs[22a] and are a = 15.162 (8) Å, b = 15.539

(19) Maheu, L. J.; Pignolet, L. J., work in progress.
(20) The solid-state magnetic susceptibility at 23 °C of $[Os_2(dtc)_6](PF_6)_2$ actually shows a slight paramagnetism ($\mu < 0.4\ \mu_B$) which is probably due to the presence of a small amount of $[Os(dtc)_3]PF_6$.
(21) Evans, D. F. *J. Chem. Soc.* **1959**, 2003.

(22) (a) The intensity data were processed as described in: "CAD4 and SDP Users Manual"; Enraf-Nonius: Delft, Holland, 1978. The net intensity I is given as

$$I = (K/\mathrm{NPI})(C - 2B)$$

where K = 20.1166 (attenuator factor), NPI = ratio of fastest possible scan rate to scan rate for the measurement, C = total count, and B = total background count. The standard deviation in the net intensity is given by

$$\sigma^2(I) = (K/\mathrm{NPI})^2[C + 4B + (pI)^2]$$

where p is a factor used to downweight intense reflections. The observed structure factor amplitude F_o is given by

$$F_o = (I/Lp)^{1/2}$$

where Lp = Lorentz and polarization factors. The $\sigma(I)$'s were converted to the estimated errors in the relative structure factors $\sigma(F_o)$ by

$$\sigma(F_o) = \tfrac{1}{2}(\sigma(I)/I)F_o$$

(b) All calculations were carried out on a PDP 11/34 computer using the Enraf-Nonius SDP programs. This crystallographic computing package is described in the following reference: Frenz, B. A. In "Computing in Crystallography"; Schenk, H., Olthof-Hazekamp, R., van Koningsveld, H., Bassi, G. C., Eds.; Delft University Press: Delft, Holland, 1978; pp 64–71.

(23) The function minimized was $\sum w(|F_o| - |F_c|)^2$ where $w = 1/\sigma^2(F_o)$. The unweighted and weighted residuals are defined as follows:

$$R = (\sum||F_o| - |F_c||)/\sum|F_o|$$

$$R_w = [(\sum w(|F_o| - |F_c|))^2/\sum w|F_o|^2]^{1/2}$$

The error in an observation of unit weight is

$$[\sum w(|F_o| - |F_c|)^2/(\mathrm{NO} - \mathrm{NV})]^{1/2}$$

where NO and NV are the number of observations and variables, respectively.

Table I. Positional and Thermal Parameters and Their Estimated Standard Deviations[a]

atom	x	y	z	β_{11}	β_{22}	β_{33}	β_{12}	β_{13}	β_{23}
Os1	0.05994 (3)	0.11048 (3)	0.27627 (4)	0.00429 (2)	0.00290 (2)	0.00363 (3)	0.00070 (4)	0.00193 (4)	0.00050 (4)
Os2	0.12881 (3)	0.29689 (3)	0.17435 (4)	0.00370 (2)	0.00278 (2)	0.00358 (3)	0.00048 (4)	0.00129 (4)	0.00060 (4)
Cl1	0.6783 (10)	0.4976 (9)	0.0455 (10)	0.0361 (15)	0.023 (1)	0.029 (1)	0.016 (2)	0.003 (3)	0.015 (2)
Cl2	0.8423 (7)	0.5611 (9)	0.1883 (9)	0.0173 (8)	0.042 (1)	0.038 (1)	−0.000 (2)	0.013 (1)	0.052 (1)
SA1	0.1142 (2)	0.0336 (2)	0.1404 (3)	0.0058 (2)	0.0033 (2)	0.0046 (2)	0.0021 (3)	0.0021 (3)	0.0016 (3)
SA2	0.1533 (3)	−0.0033 (2)	0.3471 (3)	0.0072 (2)	0.0037 (2)	0.0041 (2)	0.0029 (3)	0.0023 (3)	0.0024 (3)
SB1	−0.0738 (3)	0.0248 (3)	0.1659 (3)	0.0059 (2)	0.0043 (2)	0.0055 (2)	−0.0019 (3)	0.0029 (3)	−0.0006 (4)
SB2	−0.0436 (3)	0.0828 (3)	0.3747 (3)	0.0068 (2)	0.0068 (2)	0.0050 (2)	−0.0016 (4)	0.0046 (3)	0.0009 (4)
SC1	0.0507 (3)	0.3845 (2)	0.0471 (3)	0.0063 (2)	0.0030 (1)	0.0046 (2)	0.0005 (3)	0.0005 (3)	0.0010 (3)
SC2	0.0748 (2)	0.2040 (2)	0.0095 (3)	0.0055 (2)	0.0033 (2)	0.0040 (2)	0.0010 (3)	0.0016 (3)	0.0003 (3)
SD1	0.2471 (2)	0.4078 (2)	0.2669 (3)	0.0050 (2)	0.0040 (2)	0.0057 (2)	−0.0012 (3)	0.0015 (3)	0.0007 (3)
SD2	0.2610 (2)	0.2783 (3)	0.1102 (3)	0.0051 (2)	0.0060 (2)	0.0049 (2)	−0.0008 (3)	0.0037 (3)	−0.0007 (4)
SE1	−0.0105 (2)	0.2296 (2)	0.1823 (2)	0.0037 (1)	0.0032 (1)	0.0044 (2)	0.0006 (3)	0.0011 (3)	−0.0005 (3)
SE2	0.0656 (2)	0.3872 (2)	0.2985 (3)	0.0047 (2)	0.0032 (2)	0.0061 (2)	0.0001 (3)	0.0031 (3)	−0.0011 (3)
SF1	0.1998 (2)	0.1881 (2)	0.2866 (2)	0.0038 (1)	0.0036 (2)	0.0038 (2)	0.0010 (3)	0.0012 (3)	0.0007 (3)
SF2	0.1128 (2)	0.2073 (2)	0.4423 (3)	0.0054 (2)	0.0043 (2)	0.0043 (2)	0.0007 (3)	0.0029 (3)	−0.0000 (3)

atom	x	y	z	B, Å^2	atom	x	y	z	B, Å^2
P1	0.3105 (3)	−0.3281 (3)	0.4789 (4)	6.3 (1)	P2	0.5248 (3)	0.7710 (4)	0.1392 (4)	6.6 (1)

atom	x	y	z	β_{11}	β_{22}	β_{33}	β_{12}	β_{13}	β_{23}
F1	0.3982 (9)	−0.3810 (12)	0.4968 (11)	0.0171 (8)	0.0292 (14)	0.0212 (11)	0.029 (2)	0.025 (1)	0.030 (2)
F2	0.2194 (9)	−0.2748 (10)	0.4631 (14)	0.0105 (8)	0.0130 (11)	0.0311 (19)	0.004 (2)	0.015 (2)	0.005 (2)
F3	0.2469 (12)	−0.4068 (9)	0.4224 (12)	0.0245 (16)	0.0085 (8)	0.0180 (15)	−0.006 (2)	0.004 (3)	0.002 (2)
F4	0.3634 (11)	−0.2439 (11)	0.5337 (15)	0.0172 (12)	0.0160 (12)	0.0245 (20)	−0.014 (2)	0.004 (3)	−0.005 (3)
F5	0.3002 (8)	−0.3541 (11)	0.5824 (8)	0.0125 (7)	0.0207 (13)	0.0087 (7)	−0.005 (2)	0.013 (1)	0.003 (2)
F6	0.3183 (12)	−0.3076 (11)	0.3749 (10)	0.0238 (14)	0.0208 (13)	0.0130 (9)	0.001 (2)	0.016 (2)	0.018 (2)
F7	0.5921 (8)	0.7848 (10)	0.0746 (9)	0.0140 (7)	0.0146 (10)	0.0147 (10)	−0.010 (1)	0.016 (1)	−0.006 (2)
F8	0.4578 (9)	0.7616 (10)	0.2041 (11)	0.0226 (8)	0.0129 (11)	0.0328 (11)	−0.002 (2)	0.045 (1)	0.003 (2)
F9	0.6063 (12)	0.8071 (13)	0.2375 (13)	0.0237 (14)	0.0236 (14)	0.0154 (14)	−0.023 (2)	0.003 (2)	0.010 (2)
F10	0.4547 (10)	0.7359 (18)	0.0439 (13)	0.0176 (10)	0.0581 (27)	0.0119 (13)	−0.045 (2)	0.001 (2)	−0.008 (3)
F11	0.5000 (11)	0.8670 (11)	0.1380 (17)	0.0208 (11)	0.0144 (10)	0.0572 (25)	0.018 (2)	0.044 (2)	0.032 (3)
F12	0.5596 (12)	0.6819 (10)	0.1657 (19)	0.0191 (13)	0.0104 (10)	0.0566 (32)	0.007 (2)	0.027 (3)	0.021 (3)

atom	x	y	z	B, Å^2	atom	x	y	z	B, Å^2
NA	0.2506 (7)	−0.0758 (8)	0.2208 (9)	4.4 (3)	CD1	0.4527 (13)	0.4583 (13)	0.301 (2)	7.6 (5)
NB	−0.1961 (10)	−0.0092 (10)	0.2600 (11)	6.6 (4)	CD2	0.4641 (13)	0.3316 (14)	0.157 (2)	7.7 (5)
NC	−0.0243 (8)	0.2939 (8)	−0.1420 (9)	4.9 (3)	CD3	0.4504 (14)	0.5402 (15)	0.251 (2)	8.9 (6)
ND	0.4055 (9)	0.3839 (9)	0.2174 (10)	5.8 (3)	CD4	0.5016 (15)	0.2508 (15)	0.201 (2)	9.1 (6)
NE	−0.0956 (7)	0.3256 (7)	0.3097 (8)	3.7 (2)	CE	−0.0246 (8)	0.3156 (8)	0.275 (1)	3.3 (3)
NF	0.2821 (8)	0.2789 (8)	0.4783 (9)	4.5 (3)	CE1	−0.1748 (10)	0.2645 (10)	0.275 (1)	5.1 (3)
CA	0.1832 (8)	−0.0240 (9)	0.234 (1)	3.4 (3)	CE2	−0.1017 (9)	0.4033 (10)	0.388 (1)	4.5 (3)
CA1	0.2730 (11)	−0.0873 (12)	0.117 (1)	5.9 (4)	CE3	−0.2529 (12)	0.3040 (12)	0.194 (1)	6.8 (4)
CA2	0.3105 (11)	−0.1198 (11)	0.308 (1)	5.9 (4)	CE4	−0.0499 (11)	0.3854 (11)	0.499 (1)	5.7 (4)
CA3	0.2225 (15)	−0.1702 (15)	0.057 (2)	8.8 (6)	CF	0.2082 (8)	0.2351 (8)	0.416 (1)	3.3 (2)
CA4	0.3932 (14)	−0.0591 (15)	0.367 (2)	8.4 (6)	CF1	0.3705 (10)	0.2812 (11)	0.455 (1)	5.1 (3)
CB	−0.1170 (10)	0.0255 (10)	0.266 (1)	4.6 (3)	CF2	0.2815 (11)	0.3200 (11)	0.586 (1)	5.6 (4)
CB1	−0.2545 (14)	−0.0612 (14)	0.158 (2)	8.0 (5)	CF3	0.4313 (12)	0.2063 (13)	0.500 (1)	6.9 (5)
CB2	−0.2250 (16)	−0.0196 (16)	0.360 (2)	10.0 (7)	CC4	0.0235 (16)	0.2047 (16)	−0.283 (2)	9.7 (6)
CC	0.0268 (8)	0.2961 (9)	−0.042 (1)	3.6 (3)	CB3	−0.3248 (19)	−0.0018 (19)	0.103 (2)	12.2 (8)
CC1	−0.0758 (12)	0.3738 (12)	−0.178 (1)	6.4 (4)	CB4	−0.2917 (21)	0.0453 (21)	0.363 (3)	14.4 (10)
CC2	−0.0425 (11)	0.2101 (12)	−0.219 (1)	6.2 (4)	CF4	0.2670 (14)	0.4180 (14)	0.588 (2)	8.1 (5)
CC3	−0.1656 (13)	0.3834 (13)	−0.149 (2)	7.6 (5)	C	0.7392 (22)	0.5917 (23)	0.100 (3)	15.2 (11)
CD	0.3179 (9)	0.3622 (10)	0.201 (1)	4.4 (3)					

[a] The form of the anisotropic thermal parameter is $\exp[-(\beta_{11}h^2 + \beta_{22}k^2 + \beta_{33}l^2 + \beta_{12}hk + \beta_{13}hl + \beta_{23}kl)]$.

(6) Å, c = 13.556 (7) Å, α = 98.20 (4)°, β = 107.65 (4)°, γ = 88.57 (4)°, and V = 3012(5) Å^3. The volume of this unit cell is 108 Å^3 smaller than the one with two solvating CH_2Cl_2 molecules (vide supra). A total of 10588 unique reflections were measured in the scan range 2θ = 0–50° on an Enraf-Nonius CAD4 automatic diffractometer using graphite monochromatized Mo Kα radiation and employing a variable rate ω–2θ scan technique.[22a] No decay was noted in the intensity of three check reflections measured at intervals of 200 sequential reflections. After correction for Lorentz, polarization, background, and absorption (μ = 51.8 cm^{-1}, minimum, maximum, and average transmission factors were 0.367, 0.773, and 0.647, respectively) effects,[22] 6017 reflections (57%) were judged observed ($F_o^2 \geq 3.0\sigma(F_o^2)$) and were used in all subsequent calculations.[22b] Conventional heavy-atom techniques were used to solve the structure, and refinement, with the 2 osmium, 12 sulfur, 2 chlorine, and 12 fluorine atoms thermally anisotropic and the remaining nonhydrogen atoms isotropic by full-matrix least-squares methods (409 variables), converged R and R_w to their final values of 0.052 and 0.062, respectively.[23] The error in an observation of unit weight was 1.39 by using a value of 0.06 for p in the $\sigma(I)$ equation.[22a] In the final difference Fourier, the highest peak not within 1 Å of an osmium atom was 1.0 electron Å^{-3} and was located 1.4 Å from SE1. No new chemically reasonable features were apparent in the final difference Fourier. The asymmetric unit therefore contains the compound of formula $\{Os_2[S_2CN(C_2H_5)_2]_6\}(PF_6)_2 \cdot CH_2Cl_2$.

The final atomic coordinates with their estimated standard deviations and the final thermal parameters are given in Table I. Tables of observed and calculated structure factors, general anisotropic temperature factor expressions, and weighted least-squares planes are available (supplemental material). Figure 1 presents an ORTEP perspective of the molecular structure of the dication and shows the labeling scheme.

Results and Discussion

The synthesis of $[Os(dtc)_3]BF_4$ has been previously reported; however, only an impure compound was isolated.[1] The ex-

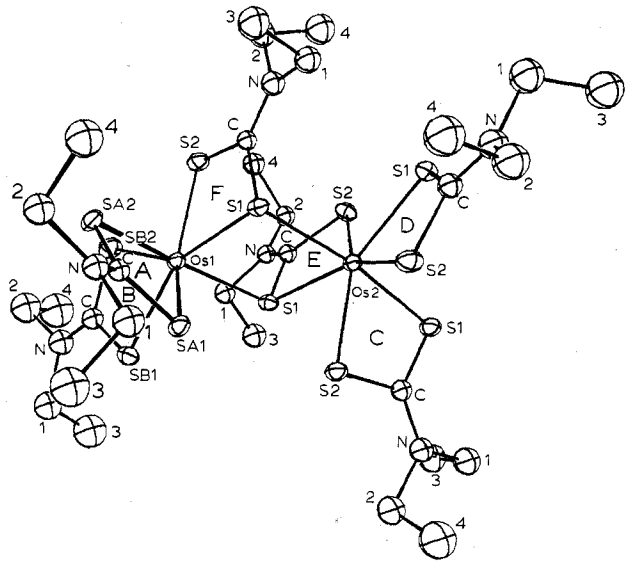

Figure 1. ORTEP drawing of the dication $[Os_2(Et_2dtc)_6]^{2+}$ showing the labeling scheme.

istence of the tris-chelated cation was primarily based on the reversible nature of the $Os(dtc)_3 \rightleftarrows [Os(dtc)_3]^+$ couple in acetone[3] and propylene carbonate[1] solution. The hexafluorophosphate salt has now been synthesized in high purity and yield and careful examination of the low-temperature ^1H NMR and electrochemistry confirms the existence of the Os(IV) cation, $[Os(dtc)_3]^+$, and also shows the presence of a monomer–dimer equilibrium in CH_2Cl_2 solution (eq 4). At

$$2[Os(dtc)_3]^+ \rightleftarrows [Os_2(dtc)_6]^{2+} \qquad (4)$$

low temperatures in CH_2Cl_2 solution the purple color of $[Os(dtc)_3]^+$ is replaced by an orange-brown color, and upon precipitation the dimer is exclusively formed. The single-crystal X-ray structure of the dimeric dication has been determined, and the molecular structure is shown in Figure 1. The coordination geometry about each osmium atom is approximately pentagonal bipyramidal (PBP) and is very similar to the geometry in $ClRu(dtc)_3$ (vide infra).

^1H NMR and Magnetic Data. The ^1H NMR spectrum of $[Os(dtc)_3]PF_6$ recorded in CD_2Cl_2 solution at ambient temperature shows isotropically shifted resonances (δ 25.03 and 3.64 ppm), thus suggesting the presence of paramagnetism. However, several additional resonances in the characteristic diamagnetic region for an ethyl group are also present. Lowering of the temperature significantly sharpens these peaks to the point where spin–spin coupling is resolved. At −34 °C the spectrum consists of two quartets and two triplets which are characteristic of two nonequivalent ethyl groups. One quartet–triplet set is shifted significantly from the usual diamagnetic position while the other is not. The relative peak areas of the two ethyl resonance patterns show a marked dependence on the concentration of $[Os(dtc)_3]^+$ as is clearly shown in Figure 2. In this figure the peaks due to the paramagnetic component are labeled M for monomer, while the diamagnetic ones are labeled D for dimer. Such a concentration dependence is expected for a monomer–dimer equilibrium. At higher osmium concentrations the amount of dimer increases relative to the amount of monomer which is consistent with eq 4. Additionally, the relative amount of dimer increases when the temperature is lowered as determined by integration of the ^1H NMR peaks and by visually observing the color of the solution which changes from purple to orange-brown as the amount of dimer increases.

The ^1H NMR resonances due to the dimeric complex $[Os_2(dtc)_6]^{2+}$ consist of only one ethyl pattern although the

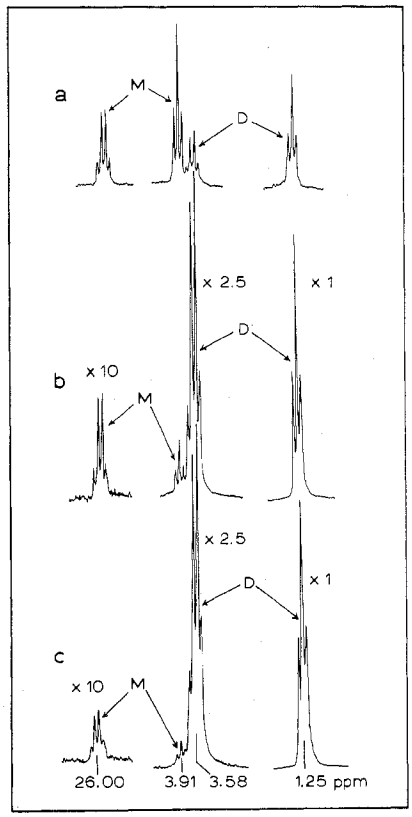

Figure 2. ^1H NMR traces of $[Os(dtc)_3]PF_6$ (M = monomer, D = dimer) recorded in CD_2Cl_2 at −34 °C as a function of osmium concentration: (a) 1.7 mM, (b) 6.8 mM, and (c) 13.3 mM. The spectra were recorded at 79.54 MHz and shifts (in ppm) relative to Me_4Si. Note that in (b) and (c) the verticle scale varies as shown by the × number.

solid-state structure of the dimer possesses nonequivalent dtc ligands. It is perhaps surprising that this complex is stereochemically nonrigid (even at −90 °C); however, $ClRu(dtc)_3$ which has a very similar coordination geometry and $ClOs(dtc)_3$ are also nonrigid.[1,5] Indeed, all of the seven-coordinate $[XM(dtc)_3]^{0,+}$ complexes known (X = CH_3CN, PPh_3, Cl, I; M = Ru or Os) except for the unusual thiocarboximido one, $ClRu(Me_2dtc)_2(SCNMe_2)$, are nonrigid in solution.[1,4,13] The mechanism of this rearrangement is unknown but probably involves fast reversible M–X bond dissociation and subsequent rearrangement of the $M(dtc)_3^+$ cation.[4] In the case of $[Os_2(dtc)_6]^{2+}$, one bridging Os–S bond could reversible rupture thereby permitting rearrangement of the short-lived six-coordinate osmium center. Osmium–S(bridge) bond rupture does indeed occur since the monomer–dimer reaction (4) has been shown to take place, although the rate of the monomer $\rightleftharpoons$ dimer reaction is slow on the ^1H NMR time scale (Figure 2). However, as the temperature is increased above ambient the monomer and dimer resonances are significantly broadened presumably due to the onset of coalescence via rapid exchange between these two species. $ClOs(dtc)_3$ is also involved in a rapid equilibrium with $[Os(dtc)_3]^+$ (vide infra).

The dimeric complex is diamagnetic in the solid state[20] as are the other PBP seven-coordinate complexes of osmium and ruthenium $[XM(dtc)_3^{0,+}$, X = Cl, PPh_3, $CH_3CN]$.[1,4] The diamagnetism presumably results from a spin-paired e_1^4 electronic configuration assuming C_{5v} local symmetry about each osmium.[4] The monomer complex is expected to be paramagnetic as is the isoelectronic and presumably isostructural iron(IV) analogue $[Fe(dtc)_3]^+$ which has magnetic data consistent with two unpaired electrons in solid and solution.[10,24] Since $[Os(dtc)_3]^+$ exists in a monomer–dimer

Table II. Low-Temperature Electrochemical Data for $Os(Et_2dtc)_3$ and $[Os(Et_2dtc)_3]^+$ [a]

complex[b]	solvent	temp, °C	process	cyclic voltammetry E_{pc}, V	E_{pa}, V	ΔE_p, mV	$(E_{pc}+E_{pa})/2$	i_{pc}/i_{pa}	dc voltammetry $E_{1/2}$, V	$E_{1/4}-E_{3/4}$, mV
$[OsL_3]^+$ [c]	CH_2Cl_2	0	$OsL_3 \rightleftharpoons OsL_3^-$	−1.066	−1.005	61	−1.035	0.98	−1.04	54
			$OsL_3^+ \rightleftharpoons OsL_3$	0.209	0.269	60	0.239	1.00	0.23	59
			$OsL_3^{2+} \rightleftharpoons OsL_3^+$	1.268	1.333	65	1.301	1.03	1.31	59
OsL_3	CH_2Cl_2	0	$OsL_3 \rightleftharpoons OsL_3^-$	−1.073	−1.014	59	−1.054	0.94	−1.05	60
			$OsL_3^+ \rightleftharpoons OsL_3$	0.205	0.262	57	0.229	1.01	0.23	52
			$OsL_3^{2+} \rightleftharpoons OsL_3^+$	1.266	1.339	73	1.302	1.08	1.31	56
OsL_3	CH_2Cl_2	−78	$OsL_3 \rightleftharpoons OsL_3^-$	−1.065	−0.91	155	−0.99	large	−1.01	95
			$OsL_3^+ \rightleftharpoons OsL_3$	0.192	0.276	84	0.234	1.01	0.26	90
$[OsL_3]^+$ [c]	CH_2Cl_2	−78	$OsL_3 \rightleftharpoons OsL_3^-$	−1.09	−0.91	180	−1.00		−1.11	115
			$OsL_3^+ \rightleftharpoons OsL_3$	0.18	0.27	94	0.23	0.82	0.23	85
			$Os_2L_6^{2+} \xrightarrow{+e^-}$?	−0.74					−0.64	150
$ClOsL_3$	$C_4H_6O_3$	0	$ClOsL_3^- \rightarrow OsL_3 + Cl^-$	−1.41						
			$ClOsL_3 \rightarrow ClOsL_3^-$	−1.25					−1.20	45
		20	$OsL_3 \rightleftharpoons OsL_3^-$	−1.11	−1.04	67	−1.08	0.97	−1.07	60
			$OsL_3^+ \rightleftharpoons OsL_3$	0.09	0.12	50	0.10	0.42	0.10	78
			$ClOsL_3^+ \rightleftharpoons ClOsL_3$	0.62	0.69	66	0.66	1.01	0.69	51

[a] All potentials are vs. SCE; potentials due to the $OsL_3^{2+} \rightleftharpoons OsL_3^+$ process are not reported at −78 °C. [b] Parent complex in solution; L = Et_2dtc. [c] Generated in situ by electrolysis of OsL_3.

equilibrium in CH_2Cl_2 solution a magnetic moment of less than 2.8 μ_B is expected. The observed moment of only 1.4 μ_B determined in CH_2Cl_2 solution at 27 °C which was 0.027 M in $[Os(dtc)_3]PF_6$ is consistent with this equilibrium.

Electrochemical Studies. $[Os(dtc)_3]^+$. The electrochemistry of $Os(dtc)_3$ in acetone (25 °C) and propylene carbonate (0 °C) solvents has been reported[1,3] and shows the presence of a four-membered electron-transfer series given in eq 5. All

$$Os(dtc)_3^- \rightleftharpoons Os(dtc)_3 \rightleftharpoons Os(dtc)_3^+ \rightleftharpoons Os(dtc)_3^{2+} \quad (5)$$

three waves are reversible by cyclic voltammetry, as judged by ΔE_p and i_{pc}/i_{pa} values.[1] Identical results are obtained by using CH_2Cl_2 solvent at 0 °C and are presented in Table II. $[Os(dtc)_3]^+$ shows the same reversible electrochemical behavior in CH_2Cl_2 solution at 0 °C (Figure 3a) as observed with $Os(dtc)_3$ (Table II), although the ^1H NMR data have established the presence of monomer–dimer equilibrium 4 (vide supra). The reversible appearance of the $Os(dtc)_3 \rightleftharpoons Os(dtc)_3^+$ couple and the absence of peaks due to $[Os_2(dtc)_6]^{2+}$ can be explained if the monomer–dimer equilibrium is established rapidly[25] and the potentials for reduction and oxidation of $[Os_2(dtc)_6]^{2+}$ are more cathodic and anodic, respectively, than for $[Os(dtc)_3]^+$.[26] In this case, only the electrochemistry of the monomer would be observed. Accordingly, a cyclic voltammogram was recorded for $[Os(dtc)_3]^+$ at −78 °C in CH_2Cl_2 solution and is reproduced in Figure 3b. The −78 °C data for this compound and for $Os(dtc)_3$ are tabulated in Table II. The cyclic voltammogram at −78 °C for $[Os(dtc)_3]^+$ clearly reveals the presence of the dimeric species. The new cathodic peak which corresponds to the reduction of $[Os_2(dtc)_6]^{2+}$ appears at E_{pc} = −0.74 V and is very similar to the cathodic peak observed for the reduction of $[(CH_3CN)Ru(dtc)_3]^+$.[4] The new peaks at potentials >0.6 V which apppear at −78 °C (Figure 3b) reveal complex nonreversible processes which have not been sorted out. The cyclic voltammogram shown in Figure 3b provides good evidence for the presence of equilibrium 4 and is therefore consistent with the ^1H NMR

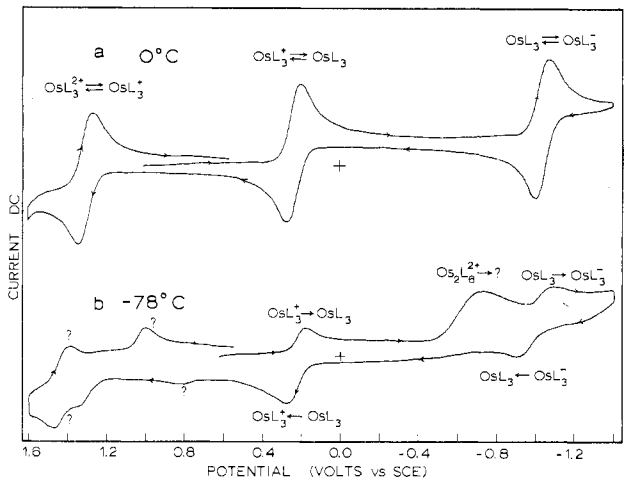

Figure 3. Cyclic voltammograms of $[Os(dtc)_3]^+$ in CH_2Cl_2 at 0 and −78 °C. The zero-current-potential position is marked by a cross (scan rate 100 and 200 mV s^{-1} for (a) and (b), respectively). The cation was generated in situ by controlled-potential electrolysis of $Os(dtc)_3$.

and magnetic results (vide supra). The striking difference between the cyclic voltammograms for $[Os(dtc)_3]^+$ recorded at 0 and −78 °C (Figure 3a,b) clearly shows the usefulness of low-temperature electrochemistry in interpreting complicated chemical behavior.

$ClOs(dtc)_3$. The cyclic voltammetry of this complex in CH_3CN solution has previously been studied and is identical with that of $[(CH_3CN)Os(dtc)_3]^+$ [2] and similar to that of $[(CH_3CN)Ru(dtc)_3]^+$.[4] The electrochemical behavior of $ClOs(dtc)_3$ in propylene carbonate solution is more complex because of the presence of equilibrium 6. Support for the

$$ClOs(dtc)_3 \rightleftarrows [Os(dtc)_3]^+ + Cl^- \quad (6)$$

presence of this equilibrium is provided by electronic absorption spectroscopy in the visible region and by low-temperature cyclic voltammetric studies (vide infra). The addition of excess chloride to an 8.8×10^{-5} M solution of $ClOs(dtc)_3$ in propylene carbonate causes a marked shift in position and intensity of the bands in the 450–600-nm range. Similar spectral changes can be caused by changing the nature of the solvent. Addition of varying amounts of water to propylene carbonate solutions

(24) Palazzotto, M. C.; Duffy, D. J.; Edgar, B. L.; Que, L., Jr.; Pignolet, L. H. *J. Am. Chem. Soc.* **1973**, *95*, 4537.
(25) Nicholson, R. S.; Shain, I. *Anal. Chem.* **1964**, *36*, 706.
(26) The potential for reduction of $[Os_2(dtc)_6]^{2+}$ is indeed more cathodic than for $Os(dtc)_3^+$ as is revealed in the −78 °C cyclic voltammogram, and the potential for oxidation is expected to be more anodic due to the increased positive charge on the dimer.

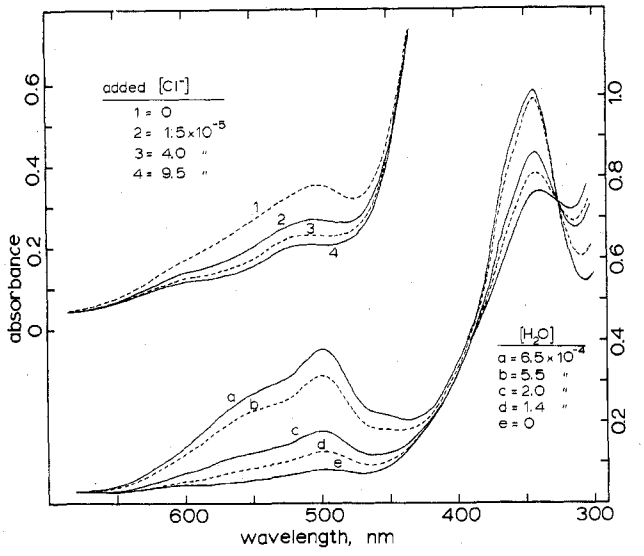

Figure 4. Electronic absorption spectra of $ClOs(dtc)_3$ in propylene carbonate solution as a function of added Cl^- via tetraethylammonium chloride and as a function of added H_2O. The concentrations of the complex remain constant during Cl^- and H_2O addition and are 8.8 × 10^{-4} and 4.4 × 10^{-5} M, respectively.

of $ClOs(dtc)_3$ causes spectral band shifts consistent with equilibrium 6. These spectral changes are shown in Figure 4. Traces 1 and e are for pure $ClOs(dtc)_3$ in propylene carbonate while trace a is similar to the spectrum of $[Os(dtc)_3]PF_6$. The addition of excess Cl^- shifts equilibrium 6 to the left whereas the addition of H_2O shifts it to the right. The observed spectral changes shown in Figure 4 provide good support for equilibrium 6. It should be noted that $Os(dtc)_3^+$ is itself in equilibrium with its dimer, $[Os_2(dtc)_6]^{2+}$, eq 4 (vide supra); however, the dimer does not absorb significantly in the 400–600-nm region.

The cyclic voltammograms of propylene carbonate solutions of $ClOs(dtc)_3$ show a marked temperature dependence and are shown in Figure 5. At 0 °C (Figure 5a), the voltammogram is complex and indicates that reaction 6 is relatively slow.[25] The wave centered at 0.66 V is reversible as determined by ΔE_p, i_{pc}/i_{pa}, and $E_{1/4} - E_{3/4}$ values (Table II) and presumably corresponds to the process $ClOs(dtc)_3 \rightleftharpoons [ClOs(dtc)_3]^+$. The irreversible anodic wave at $E_{pa} = 0.12$ V corresponds to the oxidation of $Os(dtc)_3$. This peak is more intense when longer cathodic prepolarization times are used due to the buildup of $Os(dtc)_3$ at the electrode surface. Although the return cathodic peak for the process $Os(dtc)_3^+ \rightarrow Os(dtc)_3$ is very small at 0 °C, it becomes more pronounced and nearly reversible as the temperature is increased and the rate of reaction 6 becomes fast. The wave centered at −1.08 V corresponds to the reversible process $Os(dtc)_3 \rightleftarrows Os(dtc)_3^-$. The size of this wave decreases as anodic prepolarization times are decreased. The irreversible cathodic peak at $E_{pc} = -1.25$ V is assigned to the process $ClOs(dtc)_3 \rightarrow ClOs(dtc)_3^-$ for the following reasons: (i) the peak vanishes when the temperature is increased since as reaction 6 becomes rapid[25] the amount of $ClOs(dtc)_3$ in the vicinity of the electrode decreases due to the more rapid depletion of $ClOs(dtc)_3$ (via $ClOs(dtc)_3 \rightleftarrows Os(dtc)_3^+ + Cl^- \rightarrow Os(dtc)_3 + Cl^-$) prior to reaching −1.25 V (Figure 5); (ii) addition of excess Cl^- increases the ratio, R, of this peak ($ClOs(dtc)_3 \rightarrow ClOs(dtc)_3^-$) to the one at $E_{pc} = -1.11$ V ($Os(dtc)_3 \rightarrow Os(dtc)_3^-$); (iii) addition of water decreases R; and (iv) R decreases as the anodic prepolarization time is increased. These observations also provide additional support for reaction 6. Careful examination of Figure 5a reveals a sharp increase in the cathodic current just prior to the termination of the scan at −1.4 V. This is due to another cathodic

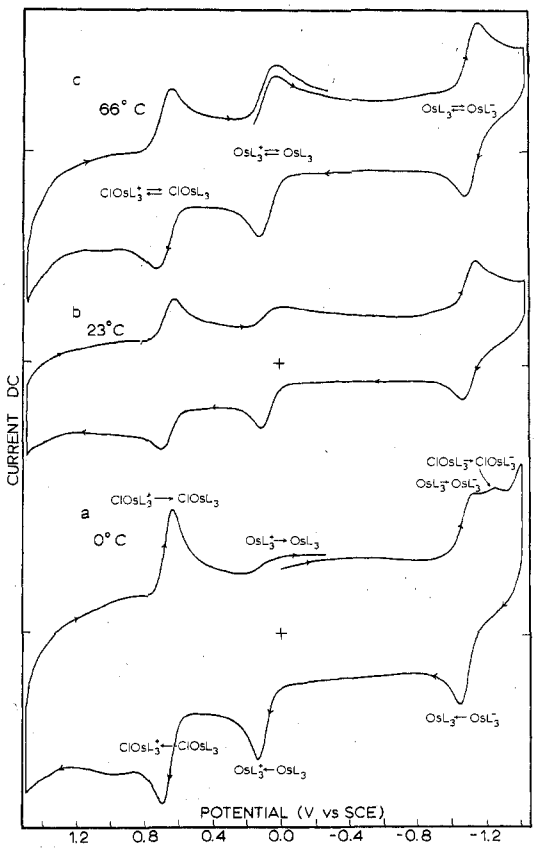

Figure 5. Cyclic voltammograms of $ClOs(dtc)_3$ in propylene carbonate solution recorded at various temperatures. The zero current positions are marked and a scan rate of 100 mV s^{-1} was used.

peak which appears at $E_{pc} = 1.41$ V (Table II). In all cases, this peak rises and falls in proportion to the magnitude of the $E_{pc} = -1.25$ V peak. This suggests that the reduction of $ClOs(dtc)_3$ takes place in two one-electron steps given in eq 7. The complete electrochemical data for $ClOs(dtc)_3$ are

$$ClOs(dtc)_3 \xrightarrow[+e^-]{E_{pc} = -1.25\ V} ClOs(dtc)_3^- \xrightarrow[+e^-]{E_{pc} = -1.41\ V} Cl^- + Os(dtc)_3^- \quad (7)$$

presented in Table II, and the various electron-transfer processes discussed above are included in Figure 5.

Structure Determination. Crystals of $[Os_2(dtc)_6](PF_6)_2 \cdot n CH_2Cl_2$, $n = 1$ or 2, were obtained by solvent diffusion from CH_2Cl_2–heptane. The crystal structures of the $n = 1$ and $n = 2$ solvates were both solved but only that of the former was completely refined (see Experimental Section). Both crystals contained the dimeric unit $[Os_2(dtc)_6](PF_6)_2$. The structure of the dication and the numbering system used throughout this paper are shown in Figure 1. The dimeric nature of the dication is evident and best appreciated in the ORTEP stereoview (Figure 6). The geometry about each Os atom is that of a distorted, pentagonal bipyramid (PBP) and is quite similar to the coordination geometry found in $ClRu(dtc)_3$, **8**,[5,27] except

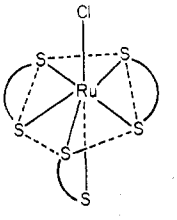

8

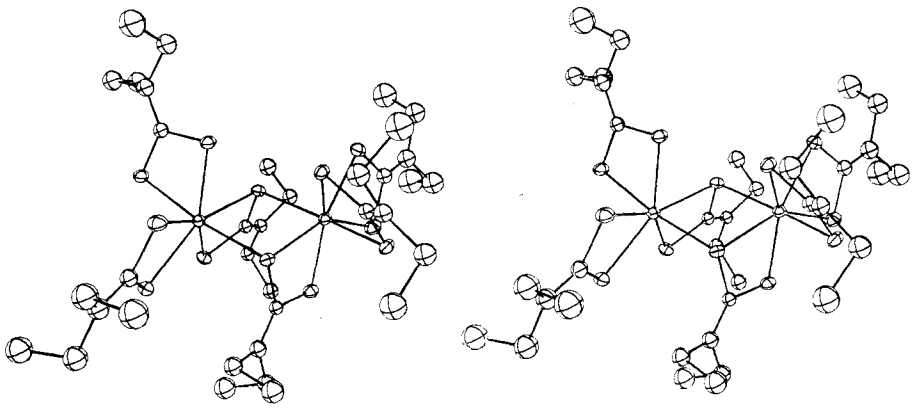

Figure 6. ORTEP stereoview of $[Os_2(Et_2dtc)_6]^{2+}$.

Table III. Selected Interatomic Distances and Angles in the Os_2S_{12} Core[a]

	Distances, Å		
Os1-SA1	2.396 (3)	Os2-SC1	2.363 (3)
Os1-SA2	2.364 (3)	Os2-SC2	2.403 (3)
Os1-SB1	2.419 (3)	Os2-SD1	2.436 (3)
Os1-SB2	2.428 (4)	Os2-SD2	2.410 (3)
Os1-SF1	2.422 (3)	Os2-SE1	2.418 (3)
Os1-SF2	2.443 (3)	Os2-SE2	2.440 (3)
Os1-SE1	2.437 (3)	Os2-SF1	2.446 (3)
SA1-SA2	2.824 (4)	SC1-SC2	2.813 (4)
SB1-SB2	2.746 (5)	SD1-SD2	2.763 (5)
SE1-SE2	2.783 (4)	SF1-SF2	2.787 (4)
SA1-SB1	2.983 (5)	SC2-SD2	2.923 (4)
SA1-SF1	2.935 (4)	SC2-SE1	2.977 (4)
SB2-SF2	2.934 (5)	SD1-SE1	2.942 (5)
SA2-SB1	3.631 (5)	SC1-SD1	3.499 (4)
SA2-SB2	3.434 (5)	SC1-SD2	3.479 (5)
SA2-SF1	3.341 (4)	SC1-SE1	3.524 (5)
SA2-SF2	3.453 (5)	SC1-SE2	3.340 (5)
SE1-SA1	3.612 (4)	SF1-SD1	3.570 (4)
SE1-SB1	3.305 (5)	SF1-SD2	3.304 (5)
SE1-SB2	3.848 (5)	SF1-SC2	3.700 (4)
SE1-SF1	3.163 (4)	SF1-SE2	3.671 (4)
SE1-SF2	3.516 (4)	Os1-Os2	3.682 (1)
	Angles, Deg		
SA1-Os1-SA2	72.8 (1)	SC1-Os2-SC2	72.4 (1)
SB1-Os1-SB2	69.0 (1)	SD1-Os2-SD2	69.5 (1)
SF1-Os1-SF2	69.9 (1)	SE1-Os2-SE2	69.9 (1)
SA1-Os1-SB1	76.6 (1)	SC2-Os2-SD2	74.8 (1)
SA1-Os1-SF1	75.0 (1)	SC2-Os2-SE1	76.3 (1)
SB2-Os1-SF2	74.1 (1)	SD1-Os2-SE2	74.2 (1)
SE1-Os1-SA1	96.7 (1)	SF1-Os2-SC2	99.4 (1)
SE1-Os1-SB1	85.8 (1)	SF1-Os2-SD1	94.0 (1)
SE1-Os1-SB2	104.5 (1)	SF1-Os2-SD2	85.7 (1)
SE1-Os1-SF1	81.2 (1)	SF1-Os2-SE1	81.1 (1)
SE1-Os1-SF2	92.2 (1)	SF1-Os2-SE2	97.4 (1)
SE1-Os1-SA2	167.0 (1)	SF1-Os2-SC1	171.6 (1)
SA2-Os1-SB1	98.8 (1)	SC1-Os2-SD1	93.6 (1)
SA2-Os1-SB2	88.5 (1)	SC1-Os2-SD2	93.6 (1)
SA2-Os1-SF1	88.6 (1)	SC1-Os2-SE1	94.9 (1)
SA2-Os1-SF2	91.8 (1)	SC1-Os2-SE2	88.1 (1)
Os1-SE1-Os2	98.6 (1)	Os1-SF1-Os2	98.3 (1)

[a] The numbers in parentheses are the estimated standard deviations of the last significant figure.

that the axial Cl atom has been replaced by a sulfur atom (of a dtc ligand) which also occupies the equatorial plane of the PBP of the other Os atom. Figure 7 shows the coordination core with the two pentagonal planes marked by dashed lines. Selected distances and angles within the coordination core are shown in Figure 7 and Table III.

The distances and angles within the PBP coordination cores about Os1 and Os2 are nearly the same within experimental

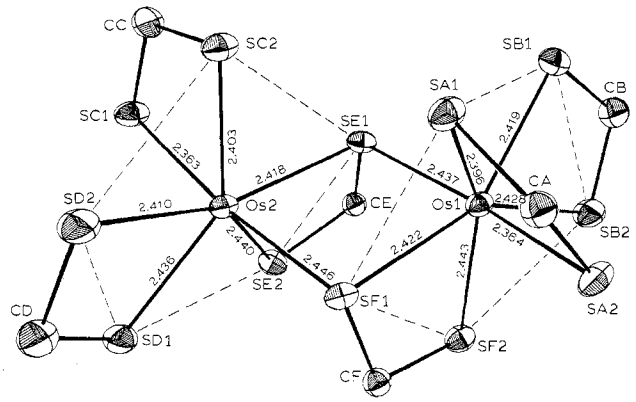

Figure 7. ORTEP drawing of the coordination core showing the pentagonal planes by dashed lines.

Table IV. Weighted Least-Square Planes

plane no.	atoms forming the plane	atoms other	distances from the plane, Å (esd)
1	SB1		0.237 (4)
	SB2		−0.118 (5)
	SF1		0.038 (3)
	SF2		0.171 (4)
	Os1		−0.007 (1)
		SA1	−0.751 (4)
2	SD1		−0.178 (4)
	SD2		−0.119 (4)
	SE1		−0.194 (3)
	SE2		0.045 (4)
	Os2		0.009 (1)
		SC2	0.784 (3)
3	Os1		0.003 (1)
	Os2		0.003 (1)
	SE1		−0.134 (3)
	SF1		−0.134 (3)
		SA2	0.442 (4)
		SC1	0.431 (4)

error and hereafter averaged values will be discussed. The values are also very similar to those within the RuS_6Cl PBP core of **8**.[5] The equatorial base of the PBP coordination core is puckered at the SA1 (or SC2) position due to the geometrical constraints imposed by the small "bite" angle of the A (or C) ligand (72.6 (1)°), compared to 90° for an ideal PBP. In addition, the S(axial)–Os–S(axial) angle of 169.3 (1)° differs somewhat from the ideal value of 180°. The S–Ru–S angles in the pentagonal base average 72.9 (1)° and are all close to the ideal PBP value of 72°, with the intraligand "bite" angles being slightly smaller (69.6 (1)°) than the interligand S–Os–S angles. Weighted least-squares planes for the pentagonal bases are shown in Table IV. The major distortion

(27) Mattson, B. M.; Pignolet, L. H. *Inorg. Chem.* **1977**, *16*, 488.

Table V. Selected Distances (Å) and Angles (Deg) in the Ligands

	ligand					
	A	B	C	D	E	F
			Distance			
S1-C	1.73 (1)	1.68 (1)	1.66 (1)	1.68 (1)	1.76 (1)	1.77 (1)
S2-C	1.71 (1)	1.70 (1)	1.73 (1)	1.71 (1)	1.71 (1)	1.67 (1)
C-N	1.32 (2)	1.30 (2)	1.34 (2)	1.32 (2)	1.30 (1)	1.32 (1)
N-C1	1.53 (2)	1.53 (2)	1.51 (2)	1.52 (2)	1.47 (2)	1.47 (2)
N-C2	1.50 (2)	1.58 (2)	1.52 (2)	1.53 (2)	1.51 (2)	1.51 (2)
C1-C3	1.51 (2)	1.49 (3)	1.53 (2)	1.52 (2)	1.54 (2)	1.54 (2)
C2-C4	1.53 (2)	1.41 (3)	1.51 (2)	1.49 (3)	1.53 (2)	1.53 (2)
			Angle			
Os-S1-C	87.1 (4)	91.4 (4)	89.2 (4)	90.3 (5)	91.4 (4)	89.9 (4)
Os-S2-C	88.5 (4)	90.6 (5)	86.4 (4)	90.6 (5)	91.8 (4)	91.5 (4)
S1-C-S2	110.4 (6)	109.0 (8)	112.0 (7)	109.4 (7)	106.9 (6)	108.2 (6)
S1-C-N	124.7 (9)	125 (1)	125 (1)	127 (1)	125.3 (9)	122.7 (9)
S2-C-N	124.9 (9)	126 (1)	123 (1)	124 (1)	127.5 (9)	129 (1)
C-N-C1	120 (1)	121 (1)	120 (1)	121 (1)	123 (1)	124 (1)
C-N-C2	121 (1)	122 (1)	122 (1)	121 (1)	121 (1)	119 (1)
C1-N-C2	118 (1)	116 (1)	118 (1)	118 (1)	116 (1)	117 (1)
N-C1-C3	105 (1)	107 (2)	111 (1)	109 (1)	111 (1)	109 (1)
N-C2-C4	108 (1)	104 (1)	110 (1)	113 (2)	110 (1)	110 (1)

Table VI. Distances (Å) in the Anions and CH_2Cl_2 Solvate[a]

P1-F1	1.52 (1)	P2-F7	1.57 (1)
P1-F2	1.56 (1)	P2-F8	1.55 (1)
P1-F3	1.54 (1)	P2-F9	1.56 (2)
P1-F4	1.52 (1)	P2-F10	1.45 (1)
P1-F5	1.57 (1)	P2-F11	1.53 (2)
P1-F6	1.53 (1)	P2-F12	1.52 (2)
C-Cl1	1.70 (3)	C-Cl2	1.76 (3)

[a] Cl1-C-Cl2 angle = 105 (2)°.

from planarity is due to the small bite angles of the dtc ligands (A and C) which span equatorial and axial positions. Therefore SA1 and SC2 are significantly out of their respective planes formed by Os and the remaining four equatorial S atoms. The dihedral angle between the two equatorial planes (plane 1 and 2 of Table IV) is 24° and these planes each have a dihedral angle of 78° with plane 3 which is formed by Os1, Os2, SE1, and SF1.

The average Os–S distance in the dication is 2.415 (3) Å compared with 2.40 (2) Å in $Os_2N(dtc)_5$[16] and 2.42 (1) Å for the dtc ligands in $[Os_2(dtc)_3(Sdtc)_2]BPh_4$[2] where Sdtc = $S_2CN(Et)_2$. The four bridging Os–S distances are similar in length; however, the ones which belong to the four-membered dtc chelate rings are shorter by ca. 7 esds. This type of a bond length difference is typical for other dtc-bridged dimers which do not contain a metal–metal bond.[28,29] The Os–Os distance is long (3.682 (1) Å) and precludes any significant metal–metal bonding. The Os–S (axial, nonbridging) distances are significantly shorter than the other Os–S distances, as has been observed in **8**.[5]

The distances between adjacent sulfur atoms in the equatorial planes are very similar and range from 2.746 (5) to 2.983 (5) Å, all of which are much shorter than the van der Waals contact distance of 3.4 Å.[5,30,31] The average interligand S–S distance along the periphery of the equatorial plane is 2.949 (4) Å which indicates that ligand–ligand interactions may be operative. Distances and angles in the dtc ligands (Table V) are normal except that the bridging S–C distances are lengthened relative to the other S–C bond lengths. There are no unusually short interionic distances and the PF_6 anions and the CH_2Cl_2 solvate molecule have normal distances and angles (Table VI).

The structure of $[Os_2(dtc)_6]^{2+}$ is quite novel and is the first example of dimerization of tris chelates into two pentagonal-bipyramidal geometries. The complex is diamagnetic as is compound **8** due to the PBP coordination geometry of each osmium atom.[2,27] The analogous iron complex $[Fe(dtc)_3]^+$ is a monomer in solid and solution and is paramagnetic ($S = 1$, d^4).[10,24] The tendency of osmium to form stronger bonds and higher coordination numbers is certainly important in the formation of the dimer.

Acknowledgment. This research was supported by Grant CHE-7821840 from the National Science Foundation. We also thank the NSF for partial support of our X-ray diffraction and structure solving equipment (NSF Grant No. CHE-7728505) and Engelhard Industries for a generous loan of OsO_4.

Registry No. $[Os_2(dtc)_6](PF_6)_2 \cdot CH_2Cl_2$, 72882-11-2; $[Os_2(dtc)_6](PF_6)_2 \cdot 2CH_2Cl_2$, 72904-40-6; $[Os(dtc)_3]PF_6$, 72882-12-3; $ClOs(dtc)_3$, 69421-31-4; $Os(dtc)_3$, 64478-70-2.

Supplementary Material Available: Listings of observed and calculated structure factor amplitudes, general temperature factor expressions, and weighted least-squares plane calculations (31 pages). Ordering information is given on any current masthead page.

(28) Hendrickson, A. R.; Martin, R. L.; Taylor, D. *Aust. J. Chem.* **1976**, *29*, 269.
(29) Hendrickson, A. R.; Martin, R. L.; Taylor, D. *J. Chem. Soc., Dalton Trans.* **1975**, 2182.
(30) van der Helm, D.; Lessor, A. E.; Merritt, L. L. *Acta Crystallogr.* **1960**, *13*, 1050.
(31) Eisenberg, R.; Ibers, J. A. *J. Am. Chem. Soc.* **1965**, *87*, 3776; *Inorg. Chem.* **1966**, *5*, 411. Eisenberg, R.; Stiefel, E. I.; Rosenberg, R. C.; Gray, H. B. *J. Am. Chem. Soc.* **1966**, *88*, 2874.